OH radical-induced oxidation in nucleosides and nucleotides unraveled by tandem mass spectrometry and IRMPD spectroscopy

Yining Jiang, Carine Clavaguéra, Suvasthika Indrajith, Chantal Houee Levin, Giel Berden, Jos Oomens, Debora Scuderi

OH Radical-Induced Oxidation in Nucleosides and Nucleotides Unraveled by Tandem Mass Spectrometry and IRMPD Spectroscopy

Yining Jiang, Carine Clavaguéra, Suvasthika Indrajith, Chantal Houée-Levin, Giel Berden, Jos Oomens and Debora Scuderi*

Dr. Yining Jiang, Dr. Carine Clavaguéra, Prof. Chantal Houée-Levin, Dr. Debora Scuderi
Université Paris-Saclay, CNRS, Institut de Chimie Physique, 91405 Orsay, France
E-mail : debora.scuderi@université-paris-saclay.fr
Homepage URL : https://www.icp.universite-paris-saclay.fr/capri/le-groupe-capri/equipes-de-recherche/couplages-sm-ir-et-ims/
https://orcid.org/0000-0003-3931-8481

Dr. Suvasthika Indrajith
Université Paris-Saclay, CNRS, Institut de Chimie Physique, 91405 Orsay, France
Stockholm University, Roslagstullsbacken 21 C, plan 4, Albano, Fysikum, 106 91 Stockholm, Sweden.

Dr. Giel Berden,
Radboud University, Institute for Molecules and Materials, FELIX Laboratory, Toernooiveld 7, Nijmegen, 6525 ED, The Netherlands

Prof. Dr. Jos Oomens
Radboud University, Institute for Molecules and Materials, FELIX Laboratory, Toernooiveld 7, Nijmegen, 6525 ED, The Netherlands
Van't Hoff Institute for Molecular Sciences, University of Amsterdam, P.O. Box 94157, Amsterdam, 1090 GD, The Netherlands

Abstract

$OH^{\bullet}$-induced oxidation products of DNA nucleosides and nucleotides have been structurally characterized by collision-induced dissociation tandem mass spectrometry (CID-MS^2) and Infrared Multiple Photon Dissociation (IRMPD) spectroscopy. CID-MS^2 results have shown that the addition of one oxygen atom occurs on the nucleobase moiety. The gas-phase geometries of +16 mass increment products of 2'-deoxyadenosine ($dA(O)H^+$), 2'-deoxyadenosine 5'-monophosphate ($dAMP(O)H^+$), 2'-deoxycytidine ($dC(O)H^+$), and 2'-deoxycytidine 5'-monophosphate ($dCMP(O)H^+$) are extensively investigated by IRMPD spectroscopy and quantum-chemical calculations. We show that a carbonyl group is formed at the C8 position after oxidation of 2'-deoxyadenosine and its monophosphate derivative. For 2'-deoxycytidine and its monophosphate derivative, the oxygen atom is added to the C5 position to form a C-OH group. IRMPD spectroscopy has been employed for the first time to provide direct structural information on oxidative lesions in DNA model systems.

1. Introduction

Reactive oxygen species (ROS), generated from both endogenous and exogenous sources (mitochondria[1], peroxisome[2], ionizing radiation, solar light[3], metal-mediated Fenton reaction[4], etc.) can cause deleterious effects by disturbing the redox balance, and then contribute to aging and age-related pathologies, such as Alzheimer diseases, cancer, and atherosclerosis[5,6]. Even though cells have developed various antioxidant defense mechanisms to recover the damages caused by ROS, a fraction of the modifications can escape from cellular defense and temporarily or permanently damage the nucleic acids in cells. Among all essential components in organisms, DNA plays a crucial role in storing and expressing biological information in the normal function of the human body. Oxidative stress in DNA has harmful consequences, such as cell death, mutations, cellular organelles dysfunction, and aging acceleration [7–11]. Therefore, there is a great interest in characterizing DNA oxidative damage induced by ROS.

In order to simulate the oxidative stress in DNA residues, ionization of water by γ-radiolysis can be employed, leading to the formation of hydroxyl radicals ($^{\bullet}$OH) in aqueous solution, which in turn oxidize water solutes [12,13]. Reactions of $^{\bullet}$OH with DNA bases are characterized by addition onto the double bonds in these molecules to give adduct radicals of bases. Subsequent reaction of base radicals leads to a variety of products from each of the DNA bases, which have been studied by gamma radiolysis or Fenton reaction in the presence of air. The radicals can either be oxidized and hydrated or reduced depending on the presence of reductants in solution. In DNA, the most susceptible site of oxidation is 2'deoxyguanosine (dG) because the guanine heterocycle has the lowest reduction potential among the four DNA bases. Oxidative damage to dG yields products that result from OH attack on C5 or C8 of the heterocyclic ring or on the 2-deoxyribose unit.

When free radicals react with the sugar moiety of DNA, sugar products and intact bases are released from DNA. It has been shown that the introduction of one phosphate group into the system decreases the rate constant of this process[14]. The rate constants of reactions between model compounds and OH radicals were determined to be close to the diffusion rate. Purine and pyrimidine bases are highly susceptible to OH radicals (rate constants 10^9-10^{10} M^{-1} s^{-1}), while the ribose phosphate moiety is less reactive (rate constant ~10^9 M^{-1} s^{-1}) [15]. Little information is available about the one-electron oxidation by OH radicals produced by gamma radiolysis in the absence of air or of reductant, which should modify the oxidation process.

The evolution of powerful MS-based characterization methods (HPLC-MS, GC-MS) paved the way to detect oxidative lesions in DNA nucleobases and related derivatives[16]. Extensive studies have been devoted to the understanding of oxidation processes in DNA components and to the chemical formula annotations of products[14,17–27]. The oxidative lesions have been mainly isolated and identified in model systems[16,27]. Although the identification and quantification of these DNA lesions have been achieved by various chromatographic methods[16,28], few studies have addressed the geometries of the oxidatively modified sites.

Recently, IRMPD spectroscopy combined with quantum-chemical calculation has emerged as a powerful tool for identifying the conformations of protonated or deprotonated DNA components[29–34] and post-translational modifications (PTM) in peptides[35]. This MS-based method involves an IR-triggered multiple-photon dissociation process occurring only at resonant vibrational frequencies, which are highly molecular-structure specific. It is therefore considered as a promising new approach for providing direct structural information on DNA damages studies by mass spectrometry.

In this work we employed IRMPD spectroscopy to investigate the one-electron oxidation of model systems generated by γ-radiation induced hydroxyl radicals ($^{\bullet}OH$) in N_2O-saturated solutions. We unravel the geometries of the final oxidation products in nucleotides and nucleosides. Investigated molecules are presented in **Figure 1.** DNA oxidation products and modified sites in molecules have been determined by Fourier Transform Ion Cyclotron Resonance-Mass Spectrometry (FT-ICR-MS) and collision-induced dissociation tandem mass spectrometry (CID-MS^2). CID-MS^2 experiments provided sequence information and helped to identify the modified sites. For the first time, IRMPD spectroscopy experiments combined with quantum-chemical calculations have been carried out to determine the diagnostic spectral features of oxidative lesions in DNA components from which detailed information of the modified sites has been obtained.

2. Results and discussion

dA and dAMP. The mass spectra of non-irradiated and irradiated solutions in a N_2O atmosphere for dA and dAMP are shown in **Figure SI2.** The most intense peaks observed in the mass spectra of non-irradiated solutions at *m/z* 252 and 332 are attributed to protonated dA and dAMP, respectively. For dA, the single oxidation product at *m/z* 268 (M+16 Da) and the double oxidation product at *m/z* 284 (+32 Da) are observed after γ-radiolysis induced oxidation. A peak at *m/z* 282 is observed as well as a result of double oxidation and dehydrogenation

(+32-2 Da). For dAMP, the same three product ions are formed and observed at m/z 348, 364, and 362, respectively. Protonated molecules and oxidation forms of dA and dAMP were mass isolated and fragmented by CID-MS^2 (**Figure SI3 and SI4).** The peaks observed in the CID-MS^2 mass spectra are listed and identified in **Table S1** and **S2**.

Protonated dA (*m/z* 252) and dAMP (m/z 332) give a typical fragment at *m/z* 136, which corresponds to AH^+. The singly oxidized products $dA(O)H^+$ and $dAMP(O)H^+$ underwent the neutral loss of a deoxyribose (-116 Da) and of deoxyribose monophosphate (-196 Da) leading to the formation of $A(O)H^+$, revealing that the oxygen addition occurs on the adenine moiety. However $[dA(O)_2\text{-}H_2]$ (*m/z* 282), shows a typical fragment at *m/z* 136, indicating that H_2 loss occurs on the sugar moiety. Based on these observations, it can be inferred that the deoxyribose moiety of dA undergoes H abstractions from the deoxyribose moiety forming $[dA\text{-}H_2]$. The addition of two oxygen atom form $[dA(O)_2\text{-}H_2]$[13]. However, the structure of this oxidation product has not been characterized by IRMPD in this present study.

In the case of $dAMP(O)_2H^+$ (*m/z* 364), the *m/z* 168 fragment shows that both oxygen atoms are added on the nucleobase moiety. The CID-MS^2 fragmentation mass spectrum of $[dAMP(O)_2\text{-}H_2]$ reveals the loss of neutral deoxyribose monophosphate (-196 Da), confirming the oxidation-induced modification occurred on the base moiety as well. This is due to the fact that the introduction of one phosphate group into the system decreases the rate constant of the process inducing the oxidation on the sugar [15].

In deuterated aqueous solution, a combined process of oxygen addition and dehydrogenation takes place. In cells, the radiation chemistry is more complex since oxygen and superoxide ions, oxidation by neighboring proteins, etc., concur in modifying the DNA. In particular, irradiation of cells by γ-radiolysis led to two main products: 8-oxo-7,8-dihydroadenine (8-oxoAde) and 4,6-diamino-5-formamidopyrimidine (Fapy-Ade) [36].

The IRMPD spectra of dAH^+ (*m/z* 252), its single oxidation product $dA(O)H^+$ (*m/z* 268) and $AdoH^+$ (*m/z* 268) are shown in **Figure 2(a)**. The IRMPD spectra of dAH^+ and $AdoH^+$ have previously been recorded by Rodgers and co-workers [37]. A peak at 1809 cm^{-1} is observed in the IRMPD spectrum of $dA(O)H^+$ compared to dAH^+. This band can be assigned to the stretching mode of a C=O group. This observation is in agreement with the structure of 8-oxoAde (M+16) in which the additional oxygen forms a carbonyl group on the adenine moiety [14,38,39]. In the hydrogen-stretching region, dAH^+ and $AdoH^+$ show three bands at 3421 cm^{-1} (intense), 3532 cm^{-1} (weak) and 3667 cm^{-1} (intense). The strong band at 3421 cm^{-1} can be assigned to the symmetric NH_2 stretching. The band observed at 3667 cm^{-1} can be ascribed to

the stretching of 3'- and 5'-hydroxyl substituents. The band at 3532 cm^{-1} is assigned to the asymmetric NH_2 stretching[38]. $AdoH^+$ shows an additional weak band at 3581 cm^{-1} assigned to the stretching mode of the hydroxyl group in position 2'. This band is not observed in the IRMPD spectrum of $dA(O)H^+$, confirming the formation of a carbonyl group after oxidation. A specific band at 3491 cm^{-1} is observed in the IRMPD spectrum of $dA(O)H^+$ in the NH/OH stretching region.

Experimental IRMPD spectra of $dAMPH^+$ and $dAMP(O)H^+$ have been recorded and compared in **Figure 2(b)** as well. In the fingerprint region, $dAMP(O)H^+$ has two extra bands at 1549 cm^{-1} and 1804 cm^{-1}, respectively compared to the protonated form. According to previous work by Rodgers and co-workers on $dAMPH^+$ and $AdoMPH^+$[32], we propose the following assignments. A diagnostic band observed at 1804 cm^{-1} for $dAMP(O)H^+$ can be attributed to the stretching mode of the carbonyl group formed after oxidation by OH radicals. In the NH/OH stretching region, two bands at 3431 cm^{-1} and 3658 cm^{-1}, respectively, arise from the symmetric NH_2 stretching and 3'- hydroxyl with P-OH stretching. The weak band at 3536 cm^{-1} of $dAMPH^+$ is assigned to NH_2 asymmetric stretching. Interestingly, the single oxidation product $dAMP(O)H^+$ shows similar bands in the NH/OH stretching region as already observed for $dA(O)H^+$, which indicates that the oxidation process is very similar to that already observed after the oxidation of dA.

DFT calculations were carried to elucidate the structures of $dA(O)H^+$ and $dAMP(O)H^+$ in the gas phase. The calculated structures for the oxo-form of dA and dAMP are referred to as dAO and dAMPO, respectively. The types of the structures ("k" for ketone forms, "e" for enol forms, and "i" for iminol forms) and an energetic ranking number are indicated in the structure nomenclature for the sake of clarity.

A comparison of the experimental and calculated spectra for the lowest energy conformers for $dA(O)H^+$ is shown in **Figure 3**. The calculated IR spectrum of the most stable structure **dAO_k1**, characterized by protonation on N3, is in good agreement with the experimental IRMPD spectrum. **dAO_k1** is stabilized by a hydrogen-bonding interaction of $N3H^+\cdots O5'$ and shows a puckered structure. Structures **dAO_k2**, **dAO_k3**, and **dAO_k4** are higher in energy compared to **dAO_k1**. They show similar IR spectra as **dAO_k1** and should be populated under our experimental conditions. The structures and spectra of possible iminol conformers (**dAO_i1**, **dAO_i2**, **dAO_i3**, **dAO_i4**) of $dA(O)H^+$ have been reported in **Figure SI5-6**. Iminol conformers can be discarded due to spectral mismatch. We therefore assign $dA(O)H^+$ to ketone conformers, and the IR band assignements of $dA(O)H^+$ are detailed in **Table S3**.

A comparison of the experimental IRMPD spectrum for dAMP(O)H^+ with calculated IR spectra of lowest energy isomers is shown in **Figure 4**. Similar to dA(O)H^+, the most stable structure, **dAMPO_k1,** exhibits a good agreement with the IRMPD spectrum. **dAMPO_k1** is protonated on the N3 atom, it has a puckered structure and it is stablized by the formation of hydrogen bond N3H^+···O2"=P. Iminol forms **dAMPO_i1** and **dAMPO_i2** are ruled out due to the lack of the prominent band at 1804 cm^{-1} and of the band at 3483 cm^{-1}. The mismatch in the NH/OH stretching region excludes **dAMPO_k2**. Structures and spectra of conformers at higher energy are displayed in **Figure SI7-8**. Detailed assignments of the observed IRMPD bands of [dAMP(O)+H]$^+$ are summarized in **Table SI4**.

dC and dCMP. The MS spectra of non-irradiated and irradiated solutions in a N_2O atmosphere for dC and dCMP, are shown in **Figures SI9(a)** and **(b)**, respectively. The peak at *m/z* 228 in the mass spectrum of dC is assigned to dCH^+ while the most intense peak in the spectrum of dCMP at *m/z* 308 is attributed to dCMPH^+. Single and double oxidation products (M+16 and M+32) are observed in both solutions. In cellular DNA, other stable oxidation products have been observed: Hyd-Ura (M+5) and Imid-Cyt, (M+50)[14] . These product ions are not observed in our experiments. The observed fragments in the CID-MS^2 mass spectra for dC, dCMP, and their oxidation products are listed and assigned in **Table SI5-6**.

According to the fragments observed in the CID-MS^2 spectra (**Figure SI10-11**), the oxidation products of dC and of dCMP show the loss of intact deoxyribose moiety (-116 Da) and of deoxyribose monophosphate (-196 Da), respectively. These observations indicate that only the nucleobase is oxidized. Previous studies performed on DNA oxidation in lymphocytes from healthy volunteers indicated the formation of 5-OHCyt [40].

A comparison of IRMPD spectra for dCH^+, dC(O)H^+ and CydH^+ is reported in **Figure 5(a)**. IRMPD spectra for dC(O)H^+ recorded at the FELIX laboratory and at the CLIO facility are clearly different. The IRMPD spectra of dC and Cyd have been previously recorded by Rodgers and co-workers [41] and are reported here for the sake of clarity. It was shown that N3 and O2 protonated tautomeric conformations coexist in the gas phase for dCH^+. In the fingerprint region, the spectrum of dC(O)H^+ recorded at FELIX laboratory shows a band at 1781 cm^{-1} which can be assigned to the C2=O stretching mode. The band at 1504 cm^{-1} in the spectrum of dC(O)H^+ recorded at the CLIO facility has a high intensity compared to the one in the spectrum recorded at the FELIX laboratory. This band can be attributed to the bending mode of a C=OH^+ group, indicating that different conformers should be populated in the two

experimental set-ups. In the NH/OH stretching region, these species have bands at 3660 cm^{-1}, 3577 cm^{-1}, 3536 cm^{-1} and 3426 cm^{-1}, respectively. The IRMPD spectrum of $dC(O)H^+$ shows an additional band at 3635 cm^{-1}, which is assigned to the OH stretching mode of the 5-OHCyt product.

The comparison of the IRMPD spectra for $dCMPH^+$ and $dCMP(O)H^+$ is reported in **Figure 5 (b)**. Spectral assignments of $dCMPH^+$ in the gas phase have been proposed by Rodgers and co-workers. [42]. In the fingerprint region, $dCMPH^+$ shows a C=O stretching band at 1774 cm^{-1}. The intensity of this band is reduced in the spectrum of $dCMP(O)H^+$. This indicates again that the addition of one oxygen atom on the base moiety changes the protonation equilibrium between N3 and O2 protonated tautomers, leading again to the formation of the $C2{=}OH^+$ form. In the NH/OH stretching region, $dCMPH^+$ and $dCMP(O)H^+$ show bands at 3426, 3532 and 3582 cm^{-1}, respectively. An extra band at 3635 cm^{-1} is observed in the IRMPD spectrum of $dCMP(O)H^+$, as well indicating the formation of an OH group on the base moiety.

A comparison of the experimental IRMPD spectrum of $dC(O)H^+$ with calculated IR spectra for the lowest energy structures is displayed in **Figure 6**. The spectrum of the most stable structure **dCO_e1** matches perfectly with the IRMPD spectrum recorded at CLIO. **dCO_e1** is protonated at the O2 position with the additional oxygen atom added at position 5 of the cytosine moiety and corresponding to the formation of the 5-OHCyt. On the contrary, the spectrum obtained at FELIX requires a combined selection of **dCO_e1** and **dCO_e2** for well assign all the observed bands. The bands at 1265 cm^{-1} and at 1792 cm^{-1} are diagnostic of the presence of **dCO_e2** structure. **dCO_e2** lies 3.2 kJ/mol higher in energy compared to **dCO_e1** and is protonated on N3 position. Both these two structures are puckered and stabilized by intramolecular hydrogen-bonding interactions. Since the energy of **dCO_e3** and **dCO_e4** are very close to that of the most stable one, they could also be populated in the gas phase. Other calculated structures with corresponding spectra are shown in **Figure SI12-13**. The presence of other structures has been excluded by energy criteria and spectral mismatch.

Based on the comparison between the experimental spectrum obtained at FELIX and the calculated spectra, the spectral assignment of the vibrational modes of $dC(O)H^+$ is detailed in **Table SI7**. The weak IR feature at ~1530 cm^{-1} is due to a combination of CN stretching, $C{=}OH^+$ stretching (for O2 protonated conformer **dCO_e1** and **dCO_e4**), C-OH bending (for N3 protonated conformer **dCO_e2** and **dCO_e3**), COH bending (for N3 protonated conformer **dCO_e2** and **dCO_e3**) and NH_2 bending modes. The bands at 1265 cm^{-1} and 1792 cm^{-1}, observed in the FELIX IRMPD spectrum can be assigned to a combination of a C=C bond in

the sugar moiety and CN and C=O stretching mode. They are diagnostic for the presence of **dCO_e2** and **dCO_e3** structures under the experimental conditions at FELIX. In the NH/OH stretching region, the sharp band at 3426 cm^{-1} is assigned to the symmetric NH_2 stretching at position 4- and NH stretching at position 3-. The band at 3536 cm^{-1} is ascribed to the asymmetric stretching of N4-H_2. The bands at 3577 cm^{-1} and 3660 cm^{-1} are assigned to the OH stretches at 2- and 5'-positions, respectively. The band at 3635 cm^{-1} is diagnostic of hydroxylation in position 5- after γ-radiolysis.

The IRMPD spectrum and the calculated vibrational spectra for the low-energy conformers of dCMP(O)H^+ are reported in **Figure 7**. The spectrum of dCMP(O)H^+ recorded at FELIX indicates a co-existence of two conformers characterized by two different protonation sites: **dCMPO_e1** and **dCMPO_e4.** The low intensity of the band at 1774 cm^{-1} for **dCMPO_e4** suggests that the abundance of this conformer is low compared to the most stable one **dCMPO_e1**. Both **dCMPO_e1** and **dCMPO_e4** are stabilized by a P=O2" ⋯ H^+O5 intramolecular hydrogen bond. **dCMPO_e1**, the most stable conformer, is protonated at the O2 position, while **dCMPO_e4** is protonated on N3. It is possible to exclude the formation of the O2 protonated conformers **dCMPO_e2** and **dCMPO_e3** in the gas phase. Other conformers higher in energy with their calculated spectra are reported in Figure **SI14-15**.

Vibrational assignments are made by comparison of the IRMPD spectrum of dCMP(O)H^+ with the spectra of selected conformers and are reported in detail in **Table S8**. The band at 1516 cm^{-1} for the O2 protonated structure is assigned to a combination of COH bending (for N3 protonated conformer **dCMPO_e4**), C=OH^+ stretching (for O2 protonated conformers **dCMPO_e1, dCMPO_e2** and **dCMPO_e3**), C-OH stretching (for O2 protonated conformer **dCMPO_e1**) and C=N stretching along with NH_2 scissoring in the base moiety as expected. The fingerprint band of N3 protonated structure at 1774 cm^{-1} is diagnostic of a neutral carbonyl stretching mode. In the NH/OH stretching region, the weak band at 3426 cm^{-1} is attributed to the symmetric stretching of N4-H_2 in **dCMPO_e1-3** and the stretching of N3-H in **dCMPO_e4**. The IR absorption at 3532 cm^{-1} is assigned to asymmetric stretching of N4-H_2. **dCMPO_e1-3** alone contributes to the medium-intensity band at 3582 cm^{-1} for the 2-hydroxyl group stretching. The sharp band at 1774 cm^{-1} represents a combined stretching mode of O3"-H and O4"-H bonds.

3.Conclusion

In this work, a combined CID-MS^2, IRMPD spectroscopy and DFT study has been carried out to shed light on the structures of the oxo-forms of nucleotides and nucleosides generated after OH radical-induced oxidation in N_2O saturated solution. The main products generated in N_2O-saturated solution of nucleotides and nucleosides after γ-radiation are from oxygen-addition onto the base moiety or correspond to dehydrogenation products, differently from a variety of modifications detected in cellular DNA by HPLC-MS^2 [27, 14].

2'-deoxyadenosine (dA), 2'-deoxyadenosine-5'-monophosphate (dAMP), 2'-deoxycytidine (dC) and 2'-deoxycytidine 5'-monophosphate (dCMP) were chosen as representative molecules for studying the geometries of oxidation products for purine and pyrimidine DNA bases.

The results of CID-MS^2 revealed that the base moiety is oxidized under our experimental conditions. Dehydrogenation has been observed to occur with the addition of oxygen atoms on the sugar moiety for dA. It is well known that the reaction of OH radical can lead to the abstraction of hydrogen atoms from the 2-deoxyribose, especially in the presence of Adenine compared to Cytosine and this mechanism is the first step in cross linking in DNA strands [13]. The hydrogen atoms abstraction yields a radical center on the sugar, especially on carbon C1', C3', C4' and C5' because these carbon atoms are directly attached to heteroatoms (nitrogen or oxygen) [43]. Oxidation can lead after the hydrogen abstraction to oxidized derivates. Different products can be formed, as a theoretical study performed on deoxyribose radicals formed by hydrogen abstraction showed that the hydrogen abstraction from carbon atoms attached to heteroatoms requires similar energies, whereas the abstraction from the C2' position is a less favourable process by 3-4 kcal/mol. M-2Da oxidation product after hydrogen abstraction can lead to oxidation products resulting from one or more oxygen atoms [44].

When free radicals react with the sugar moiety of DNA, sugar products and intact bases can be released from DNA, as observed for dA in our oxidation conditions. It has been shown that the introduction of one phosphate group into the system decreases the rate constant of the process. For $[dAMP(O_2)\text{-}H_2 + H]^+$ the oxygen atoms are added on the base moiety. This is the reason why in the case of dA the observed double oxidation in our experimental conditions is located on the sugar moiety and in the case of dAMP is more located on the DNA base [14,15].

By combining the IRMPD spectra with DFT calculation, the diagnostic IRMPD signature of the C=O bond formation in dA(O) and dAMP(O) at ~1800 cm^{-1} has been identified for the first time. These observations confirm that the oxidation occurred in the adenine moiety by

formation of a new carbonyl group at the 8-position. The protonation site of both $dA(O)H^+$ and $dAMP(O)H^+$ was shown to be at the N3 atom.

The presence of the intense band at ~1530 cm^{-1} for C-OH vibrations of cytosine moiety and the band at ~1790 cm^{-1} for C=O stretching in dC(O) and dCMP(O) showed the co-existence of N3 and O2 protonated conformers with the formation of an O5-H group after radiolysis-induced oxidation and tautomerization in the gas phase.

For **dC,** DFT calculations showed that the spectrum of the most stable structure **dCO_e1** matches perfectly with the IRMPD spectrum recorded at CLIO facility. **dCO_e1** is protonated at the O2 position with the additional oxygen atom added at position 5 of the cytosine moiety and corresponding to the formation of the 5-OHCyt. On the contrary, the spectrum obtained at FELIX requires a combined selection of **dCO_e1** and **dCO_e2** for well assign all the observed bands. The bands at 1265 cm^{-1} and at 1792 cm^{-1} are diagnostic of the presence of **dCO_e2** structure. The ionization sources in the two experiments are similar, ESI sources in both cases, but we should also keep in mind that the source geometries are quite different. In the Amazon ion trap (in Felix Facility) the ESI source is an in-axis source and in the case of the FT-ICR mass spectrometer (in CLIO Facility) is off-axis source. We kept the experimental conditions for sample preparation, oxidation, mass spectrometry and IRMPD spectroscopy experiments very similar in CLIO and Felix but the ESI parameters should be adapted in each case to optimize the ion signal. In particular we do not know the ion temperature in the sources which should be an important parameter for isomer formation [45]. We should also stress on the fact that the mass spectrometers used to record the IRMPD spectra are not the same and we cannot exclude a priori that some isomerisation could occur during the ion transfer.

IRMPD spectroscopy provides specific diagnostic signatures to identify the oxidation products and has been applied here for the first time to determine the structure of products resulting from oxidative damage of model DNA systems. Indeed, IRMPD spectroscopy, combined with quantum chemical calculation, is a powerful structural tool to provide direct information of geometric details on the modified sites of DNA model systems, which was not available from traditional detection techniques. These results pave the ways to further investigations on more complex DNA model systems by IRMPD spectroscopy. In particular further investigations will be performed to characterize the structure of the double oxidized products of dA and dAMP and their $-H_2$ products.

Experimental section

Materials. All reagents were purchased from Sigma Aldrich and used without further purification. N_2O was delivered by ALPHA GAZ with a purity of 99.998%. The stock solution was prepared in deionized water from a Millipore system in 10^{-3} M.

Sample preparation. γ-irradiations were carried out using the panoramic ^{60}Co γ-source IL60PL Cis-Bio International (France) in the Paris-Saclay University (Orsay, France). The dose rate was determined by Fricke dosimetry[46]. Samples were gently purged while stirring under a N_2O atmosphere for approximately 30 min before irradiation. All irradiations were performed at room temperature. The chosen oxidant species was the hydroxyl radical $^{\bullet}OH$ produced by γ- radiolysis of N_2O-saturated aqueous solutions. [47]:

$$H_2O \rightarrow {}^{\bullet}OH, H^{\bullet}, e^{-}_{aq}, H_2, H_2O_2, H^{+}, OH^{-} \qquad (1)$$

$$e^{-}_{aq} + N_2O + H_2O \rightarrow {}^{\bullet}OH + OH^{-} + N_2 \qquad (2)$$

The radiation chemical yield (G) is equal to 0.55 μmol J^{-1} (equations 1 and 2). H atoms are also created in much lower yield (0.05 μmol J^{-1}), which lead to desulfuration of methionine. The H_2O_2 yield is also lower (0.07 μmol J^{-1}). Samples were irradiated with a total dose of 1517 Gy for dA and dAMP, and of 1080 Gy for the rest. Experiments were performed at room temperature.

CID-MS^2. All the MS and CID-MS^2 operations have been performed using a 7 T hybrid FT-ICR mass spectrometer (Bruker, APEX-Qe)[48] at CLIO Facility in Orsay, France. Samples were diluted to 50 μM in a mixture of 50/50 (v/v) water/methanol containing 0.1% formic acid for enhancing the protonation. Analytes were introduced by an external ESI nebulizer, assisted by a 120 μL/h syringe pump. MS spectra before and after irradiation were then recorded and compared for identifying the radiolysis-induced products.

As for CID-MS^2 operation, the selected ions (with an isolatiton window of 2 Da) were fragmented by colliding with Ar in a hexapole collision cell. Fragments were pulse extracted and finally detected in the ICR analyzer cell.

IRMPD spectroscopy. IRMPD spectroscopy experiments were carried out both at the FELIX laboratory[49] in Nijmegen (The Netherlands) and at the CLIO facility[50] in Orsay (France). Sample solutions (10 μM) for electrospray ionization (ESI) were prepared in mixtures of 50/50 (v/v) water/methanol containing 0.1% formic acid for ESI-(+) positive mode. At FELIX, the IRMPD spectra were measured with a modified three-dimensional quadrupole ion trap mass

spectrometer (Bruker, AmaZon Speed ETD) coupled to the FELIX infrared free electron laser (FEL) beamline. The set-up has been described in detail elsewhere [51]. The analyte solution was nebulized, desolvated and ionized via electrospray ionization (ESI) with a flow rate of 120 μL/h assisted by pressurized N_2 nebulizing gas at 180-220 ℃. The spray voltage was 4 kV. Ions of interest were accumulated, isolated by MS/MS selection and then irradiated by a single FEL macropulse in the fingerprint region (800-2000 cm^{-1}). The FEL fires at 10 Hz with macropulses of 5-10 μs (bandwidth of ~0.4% of the center frequency and energy of 40-100 mJ/pulse), which consist of a train of 6 ps micropulses spaced by 1 ns. The IR induced fragmentation yield at each IR frequency step was obtained from an average of 6 mass spectra. At the CLIO facility, ion spectra were obtained by using a 7 T hybrid FT-ICR mass spectrometer (Bruker, APEX-Qe)[48] coupled to the CLIO IR FEL for the fingerprint region or to the OPO/OPA system (Laser Vision) for the hydrogen stretching region. An auxiliary CO_2 laser (Universal Laser System, 10 W, cw operation centered at λ = 10.6 μm) was added to enhance the on-resonance fragmentation yield. The IR-FEL output of CLIO consists of 8 μs long macropulses fired at a repetition rate of 25 Hz, and each macropulse is formed by about 500 micropulses of ~1 ps/pulse. Micropulses are spaced by 16 ns at CLIO. The energy of macropulse is around 30-60 mJ. Similar to FELIX, the spectral width is ~0.5% of the central wavelength[52]. The plot of Felix and Clio energies as function of the wavelength is reported in SI1. In the 3300-3800 cm^{-1} range, the OPO/OPA system delivers 10-20 mJ/pulse (6 ns pulse duration, bandwidth 3 cm^{-1}, 10 Hz repetition rate). In the FT-ICR MS, ions were isolated, thermalized and pulse extracted to the FT-ICR cell ($<10^{-9}$ mbar) for interacting with the IR radiation.

The IRMPD spectra are obtained by recording the photofragmentation yield, $R = -\ln[I_p/(I_p+\Sigma I_f)]$ as a function of the wavenumber of the IR radiation, with I_p and I_f the precursor and fragment ion intensities in the mass spectrum. The IR yield has been linearly corrected for the frequency-dependent variation of the laser pulse energy[53].

DFT calculations. Calculations have been carried out for dAH^+, $dAMPH^+$, dCH^+ and $dCMPH^+$. According to the previous studies on the protonation sites of nucleosides and nucleotides, the most favorable sites of protonation, N3 for dAH^+ and $dAMPH^+$[31,32], N3 and O2 for dCH^+ (Figure 1) and $dCMPH^+$[34], were taken into consideration for simulating the geometries. Based on the chemical formula proposed for the +16 Da mass increment products of DNA bases[14], an oxygen atom was added at the 8-position in adenine moiety[36] and at the 5- position in

cytosine moiety[54] to form a carbonyl group and hydroxyl substituent for constructing the structures of singly oxidized forms, respectively.

Conformations have been explored extensively. The iterative metadynamic sampling and genetic crossover (iMTD-GC) method implemented in the Conformer Rotamer Ensemble Sampling Tool (CREST) program[55,56] have been used for the conformer sampling. The sampling included additional geometry optimizations of the final conformer ensemble. The calculations of the conformer energies were based on the semi-empirical extended tight-binding method (GFN2-xTB)[57]. Possible tautomeric forms of these conformers have been examined as well. Geometry optimizations, IR spectral simulations and energy calculations were carried out at the B3LYP/6-311+G(2d, 2p) level of theory with the Gaussian16 package of programs [58].

Dual-scaling factors have been applied for a better agreement between the theoretical spectra and the experimental ones[59]: 0.98 in the fingerprint region and 0.95 in the hydrogen stretching region. In addition, particularly, for nucleotides with a monophosphate group, calculated frequencies associated with phosphate group were kept unscaled [29,30,60]. The calculated frequencies were convoluted with a 20 cm^{-1} (10 cm^{-1}) full width at half maximum (FWHM) Lorentzian line shape function in the fingerprint region (OH/NH stretching region). Spectral assignments have been achieved by comparing the experimental and computed IR spectra.

Acknowledgements

The mass spectrometry SMAS platform staff at the Institut de Chimie Physique (ICP) in Paris-Saclay University, J.M. Ortega and B. Redlich are gratefully acknowledged. We also thank the CLIO and FELIX facilities and the technical staffs, in particular Nicolas Jestin, Victor Claessen, Marije Barel, Wouter Stumpel and Bryan Willemsen for their efficient assistance during the IRMPD experiments. DS and YJ thank Erna Gouwens from FELIX office for her assistance.

This research was fund by the EU Horizon 2020 Programme (EU_FT - ICR_MS) under grant agreement No 731077. Financial support from the IR INFRANALYTICS FR2054 for conducting the research is gratefully acknowledged. The research leading to these results has received funding from LASERLAB-EUROPE (grant agreement no. 871124, European Union's Horizon 2020 research and innovation programme). We gratefully acknowledge the Nederlandse Organisatie voor Wetenschappelijk Onderzoek (NWO) for the support experiments performed at the FELIX Laboratory.

Keywords: Ab initio calculations, DNA Nucleosides and Nucleotides, IRMPD spectroscopy, Mass spectrometry, OH-induced Oxidation.

Reference

[1] E. Cadenas, K. J. Davies, *Free Radic Biol Med* **2000**, *29*, 222.
[2] K. Okumoto, S. Tamura, M. Honsho, Y. Fujiki, *Adv Exp Med Biol* **2020**, *1299*, 3.
[3] J. Cadet, T. Douki, J.-L. Ravanat, P. D. Mascio, *Photochem. Photobiol. Sci.* **2009**, *8*, 903.
[4] S. Frelon, T. Douki, A. Favier, J. Cadet, *J. Chem. Soc., Perkin Trans. 1* **2002**, 2866.
[5] B. N. Ames, L. S. Gold, *Mutat Res* **1991**, *250*, 3.
[6] B. N. Ames, M. K. Shigenaga, T. M. Hagen, *Proc Natl Acad Sci U S A* **1993**, *90*, 7915.
[7] M. Valko, M. Izakovic, M. Mazur, C. J. Rhodes, J. Telser, *Mol Cell Biochem* **2004**, *266*, 37.
[8] M. Valko, D. Leibfritz, J. Moncol, M. T. D. Cronin, M. Mazur, J. Telser, *Int J Biochem Cell Biol* **2007**, *39*, 44.
[9] M. D. Evans, M. Dizdaroglu, M. S. Cooke, *Mutat Res* **2004**, *567*, 1.
[10] B. Halliwell, C. E. Cross, *Environ Health Perspect* **1994**, *102*, 5.
[11] B. Halliwell, *Biochem J* **2007**, *401*, 1.
[12] C. von Sonntag, *Free-Radical-Induced DNA Damage and Its Repair*, Springer, Berlin, Heidelberg, **2006**.
[13] C. von Sonntag, *The Chemical Basis of Radiation Biology*, Taylor & Francis, London; New York, **1987**.
[14] J. Cadet, J. R. Wagner, *Cold Spring Harb Perspect Biol* **2013**, *5*, DOI 10.1101/cshperspect.a012559.
[15] S. Steenken, *Chem. Rev.* **1989**, *89*, 503.
[16] J. Cadet, T. Douki, J.-L. Ravanat, *Mutat Res* **2011**, *711*, 3.
[17] H. Kasai, S. Nishimura, *Nucleic Acids Res* **1984**, *12*, 2137.
[18] H. G. Claycamp, K.-K. Ho, *Int. J. Rad. Biol.* **1993**, *63*, 597.
[19] H. Kasai, Z. Yamaizumi, M. Berger, J. Cadet, *J. Am. Chem. Soc.* **1992**, *114*, 9692.
[20] J.-L. Ravanat, R. J. Turesky, E. Gremaud, L. J. Trudel, R. H. Stadler, *Chem. Res. Toxicol.* **1995**, *8*, 1039.
[21] T. Douki, J.-L. Ravanat, J.-P. Pouget, I. Testard, J. Cadet, *Int. J. Rad. Biol.* **2006**, *82*, 119.
[22] J.-L. Ravanat, C. Saint-Pierre, J. Cadet, *J. Am. Chem. Soc.* **2003**, *125*, 2030.
[23] A.-G. Bourdat, T. Douki, S. Frelon, D. Gasparutto, J. Cadet, *J. Am. Chem. Soc.* **2000**, *122*, 4549.
[24] T. Douki, J. Rivière, J. Cadet, *Chem. Res. Toxicol.* **2002**, *15*, 445.
[25] J.-L. Ravanat, P. D. Mascio, G. R. Martinez, M. H. G. Medeiros, J. Cadet, *J. Biol. Chem.* **2000**, *275*, 40601.
[26] O. R. Alshykhly, A. M. Fleming, C. J. Burrows, *J. Org. Chem.* **2015**, *80*, 6996.
[27] J. Cadet, T. Douki, J.-L. Ravanat, *Free Radic. Biol. Med.* **2010**, *49*, 9.
[28] J. Cadet, T. Douki, J.-L. Ravanat, J. R. Wagner, *Bioanal Rev* **2012**, *4*, 55.
[29] Y. -w. Nei, N. Hallowita, J. D. Steill, J. Oomens, M. T. Rodgers, *J. Phys. Chem. A* **2013**, *117*, 1319.
[30] Y. -w Nei, K. T. Crampton, G. Berden, J. Oomens, M. T. Rodgers, *J Phys Chem A* **2013**, *117*, 10634.

[31] R. R. Wu, B. Yang, G. Berden, J. Oomens, M. T. Rodgers, *J. Phys. Chem. B* **2015**, *119*, 2795.
[32] R. R. Wu, C. C. He, L. A. Hamlow, Y.-W. Nei, G. Berden, J. Oomens, M. T. Rodgers, *J Phys Chem B* **2016**, *120*, 4616.
[33] J.-Y. Salpin, S. Guillaumont, J. Tortajada, L. MacAleese, J. Lemaire, P. Maitre, *ChemPhysChem* **2007**, *8*, 2235.
[34] R. R. Wu, L. Hamlow, C. C. He, Y. -w Nei, G. Berden, J. Oomens, M. Rodgers, *J. of Am. Soc. Mass Spectrom.* **2017**, DOI 10.1007/s13361-017-1653-8.
[35] P. Maitre, D. Scuderi, D. Corinti, B. Chiavarino, M. E. Crestoni, S. Fornarini, *Chem. Rev.* **2020**, *120*, 3261.
[36] J.-P. Pouget, S. Frelon, J.-L. Ravanat, I. Testard, F. Odin, J. Cadet, *Radiat Res* **2002**, *157*, 589.J.
[37] R. R. Wu, B. Yang, G. Berden, J. Oomens, M. T. Rodgers, *J. Phys. Chem. B* **2015**, *119*, 2795.

[38] J. Cadet, T. Douki, J.-L. Ravanat, *Acc Chem Res* **2008**, *41*, 1075.
[39] J. Cadet, T. Douki, J.-L. Ravanat, *Free Radic. Biol. Med.* **2010**, *49*, 9.
[40] K. J. Lenton, H. Therriault, T. Fülöp, H. Payette, J. R. Wagner, *Carcinogenesis* **1999**, *20*, 607.
[41] R. R. Wu, B. Yang, C. E. Frieler, G. Berden, J. Oomens, M. T. Rodgers, *J. Phys. Chem. B* **2015**, *119*, 5773.

|42] R. R. Wu, L. A. Hamlow, C. C. He, Y. -w. Nei, G. Berden, J. Oomens, M. T. Rodgers, *J. Am. Soc. Mass Spectrom.* **2017**, *28*, 1638.

[43] A. Matros, D. Peshev2, M. Peukert, H.-P. Mock and W. Van den Ende, *Plant J.* **2015**, 82, 822–839

[44] K. Miaskiewicz and R. Osman, *J. Am. Chem. Soc.* **1994**, 116, 232-238

[45] D. Morsa, V. Gabelica, F. Rosu,J. Oomens and E. De Pauw, *J. Phys. Chem. Lett.* **2014**, 5, 3787−3791

[46] W. T. Spinks, R. J. Woods, *An Introduction to Radiation Chemistry*, Wiley-Interscience, New York, **1990**.
[47] V. Kadlcik, C. Sicard-Roselli, C. Houée-Levin, M. Kodicek, C. Ferreri, C. Chatgilialoglu, *Angew. Chem. Int. Ed.* **2006**, *45*, 2595.
[48] J. M. Bakker, T. Besson, J. Lemaire, D. Scuderi, P. Maître, *J. Phys. Chem. A* **2007**, *111*, 13415.
[49] D. Oepts, A. F. G. van der Meer, P. W. van Amersfoort, *Infrared Phys. Technol.* **1995**, *36*, 297.
[50] R. Prazeres, F. Glotin, C. Insa, D. A. Jaroszynski, J. M. Ortega, *Eur. Phys. J. D* **1998**, *3*, 87.
[51] J. Martens, G. Berden, C. R. Gebhardt, J. Oomens, *Rev. S. Instrum.* **2016**, *87*, 103108.

[52] F. Glotin, J. M. Ortega, R. Prazeres, C. Rippon, *Nucl. Instrum. Meth. B* **1998**, *144*, 8.
[53] G. Berden, M. Derksen, K. J. Houthuijs, J. Martens, J. Oomens, *Int. J. Mass Spectrom.* **2019**, *443*, 1.
[54] S. Tremblay, J. R. Wagner, *Nucleic Acids Res* **2008**, *36*, 284.

[55] P. Pracht, F. Bohle, S. Grimme, *Phys. Chem. Chem. Phys.* **2020**, *22*, 7169.
[56] Conformer-rotamer ensemble sampling tool based on the xtb semiempirical extended tight-binding program package crest. https://github.com/grimme-lab/crest.
[57] C. Bannwarth, S. Ehlert, S. Grimme, *J. Chem. Theory Comput.* **2019**, *15*, 1652.
[58] "Gaussian 16, Revision B.01, Frisch, M.J., Trucks, G.W., Schlegel, H.B., Scuseria, G.E., Robb, M.A., Cheeseman, J.R.; Scalmani, G.; Barone, V.; Petersson, G.A.; Nakatsuji, H.; Li, X.; Caricato, M.; Marenich, A.V.; Bloino, J., Janesko, B.G., Gomperts, R., Mennucci, B., Hratchian, H.P., Ortiz, J.V., Izmaylov, A.F., Sonnenberg, J.L., Williams-Young, D., Ding, F., Lipparini, F., Egidi, F., Goings, J., Peng, B., Petrone, A., Henderson, T., Ranasinghe, D., Zakrzewski, V.G., Gao, J., Rega, N., Zheng, G., Liang, W., Hada, M., Ehara, M., Toyota, K., Fukuda, R., Hasegawa, J., Ishida, M., Nakajima, T., Honda, Y., Kitao, O., Nakai, H., Vreven, T., Throssell, K., Montgomery Jr., J.A., Peralta, J.E., Ogliaro, F., Bearpark, M.J., Heyd, J.J., Brothers, E.N., Kudin, K.N., Staroverov, V.N., Keith, T.A., Kobayashi, R., Normand, J., Raghavachari, K., Rendell, A.P., Burant, J.C., Iyengar, S.S., Tomasi, J., Cossi, M., Millam, J.M., Klene, M., Adamo, C., Cammi, R., Ochterski, J.W., Martin, R.L., Morokuma, K., Farkas, O., Foresman, J.B., Fox, D.J. Gaussian, Inc., Wallingford CT (2016) GaussView 5.0. Wallingford, E.U.A. - References - Scientific Research Publishing," can be found under https://www.scirp.org/(S(lz5mqp453ed%20snp55rrgjct55))/reference/referencespapers.aspx?referenceid=2418053, **n.d.**
[59] M. D. Halls, J. Velkovski, H. B. Schlegel, *Theor. Chem. Acc.* **2001**, *105*, 413.
[60] D. Scuderi, C. F. Correia, O. P. Balaj, G. Ohanessian, J. Lemaire, P. Maitre, *ChemPhysChem* **2009**, *10*, 1630.

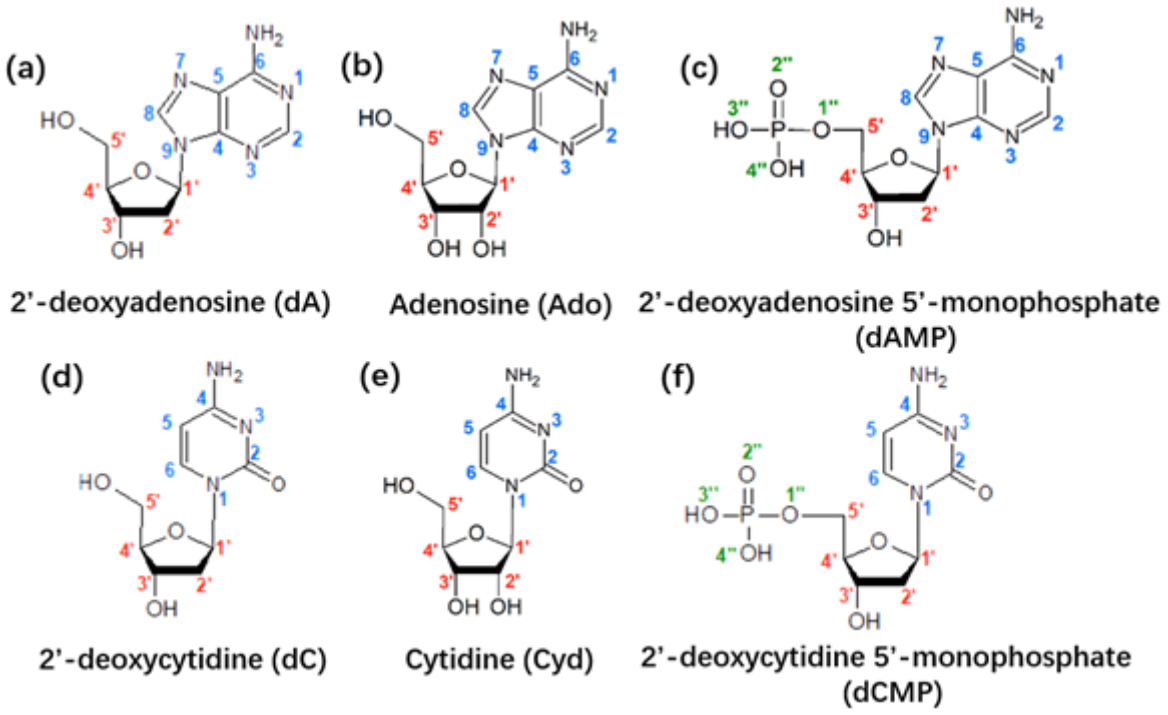

Figure 1. Chemical structures of **(a)** 2'-deoxyadenosine (dA, MW=251 g.mol^{-1}), **(b)** adenosine (Ado, MW=267 g.mol^{-1}) and **(c)** 2'-deoxyadenosine 5'-monophosphate (dAMP, MW=331 g.mol^{-1}); **(d)** 2'-deoxycytidine (dC, MW=227 g.mol^{-1}), **(e)** cytidine (Cyd, MW=243 g.mol^{-1}) and **(f)** 2'-deoxycytidine 5'-monophosphate (dCMP, MW=307 g.mol^{-1}).

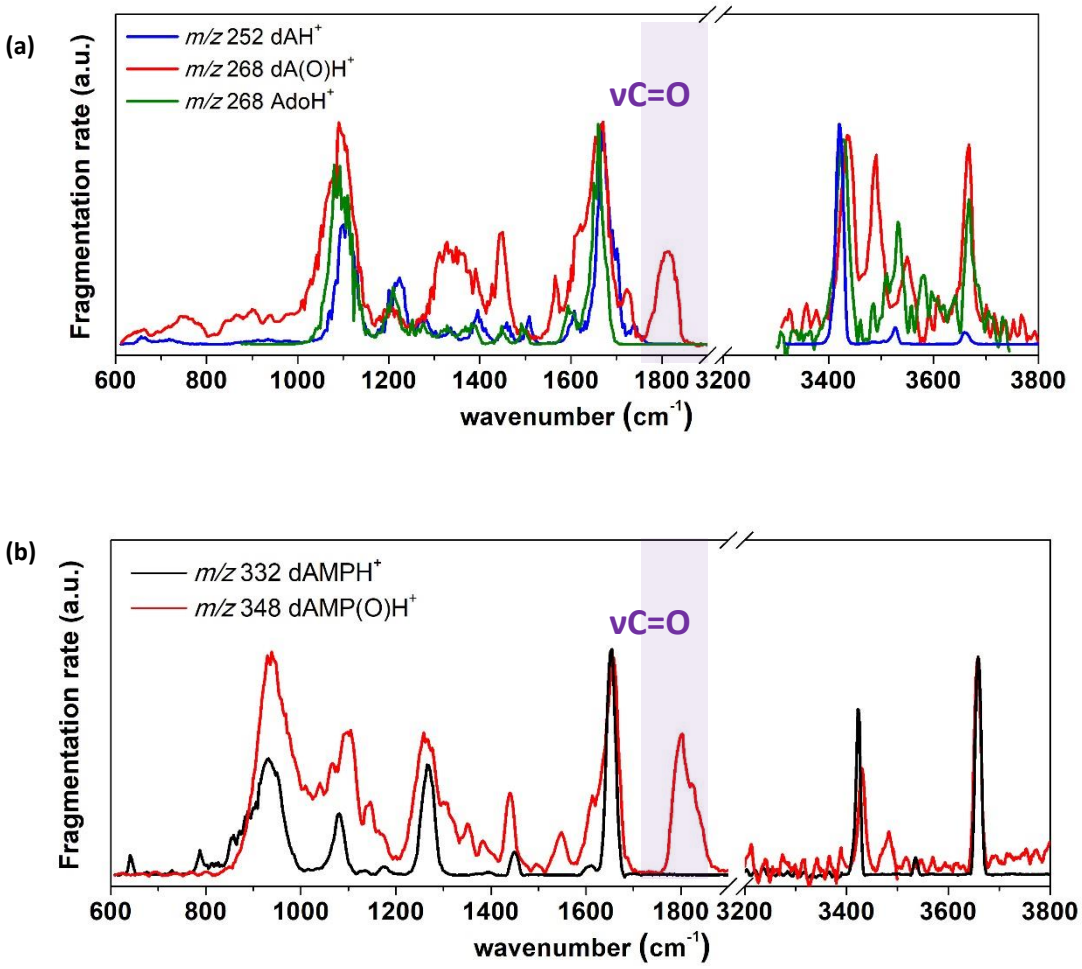

Figure 2. Comparison between the IRMPD spectra **(a)** of dAH^+ (blue), $AdoH^+$(green) and of single oxidation product $dA(O)H^+$ (red); **(b)** of $dAMPH^+$ (black) and its single oxidation product $dAMP(O)H^+$ (red).

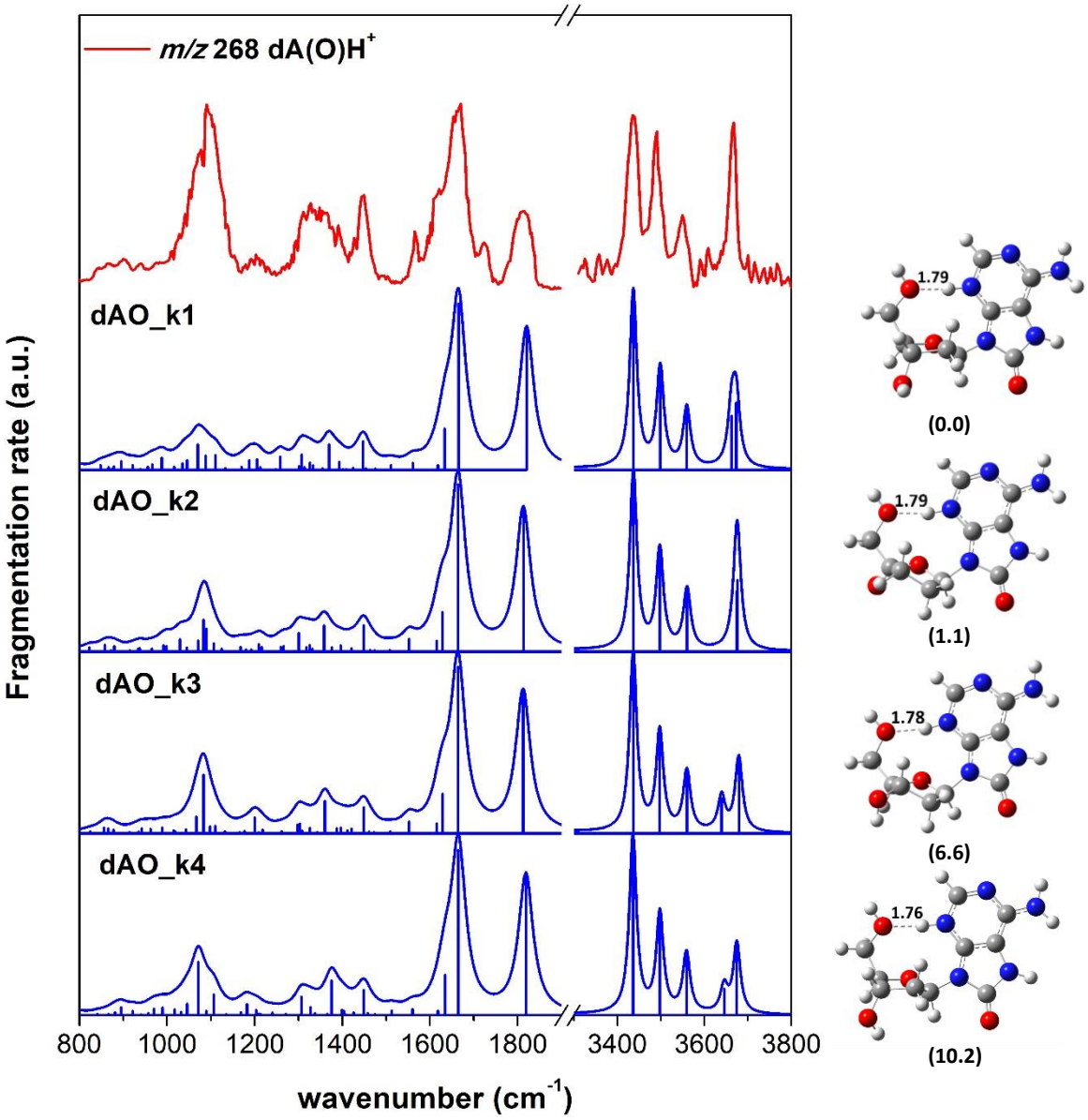

Figure 3. Comparison of the experimental IRMPD spectra for $dA(O)H^+$ with convoluted calculated IR absorption spectra of representative conformers of the lowest energies optimized at the B3LYP/6-311+G(2d,2p) level of theory. The H-bond distances are in Å. The corresponding structures are reported on the right. The relative Gibbs free energy (ΔG) at 298 K is given in parentheses and is expressed in kJ/mol.

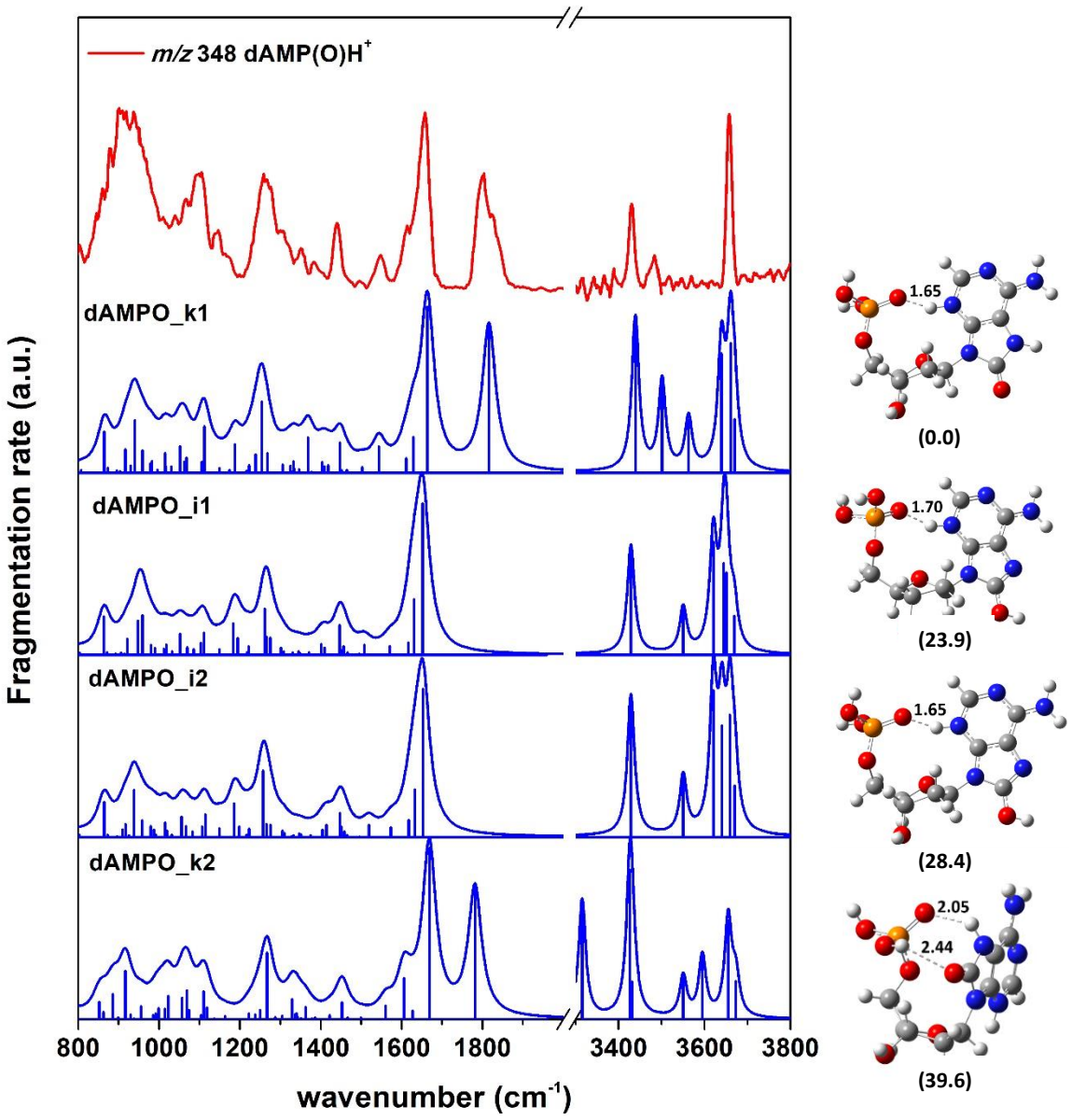

Figure 4. Comparison of the experimental IRMPD spectra for dAMP(O)H^+ with convoluted calculated IR absorption spectra of representative conformers of the lowest energies optimized at the B3LYP/6-311+G(2d,2p) level of theory. The H-bond distances are in Å. The corresponding structures are reported on the right. The relative Gibbs free energy (ΔG) at 298 K, in parentheses, is given in kJ/mol.

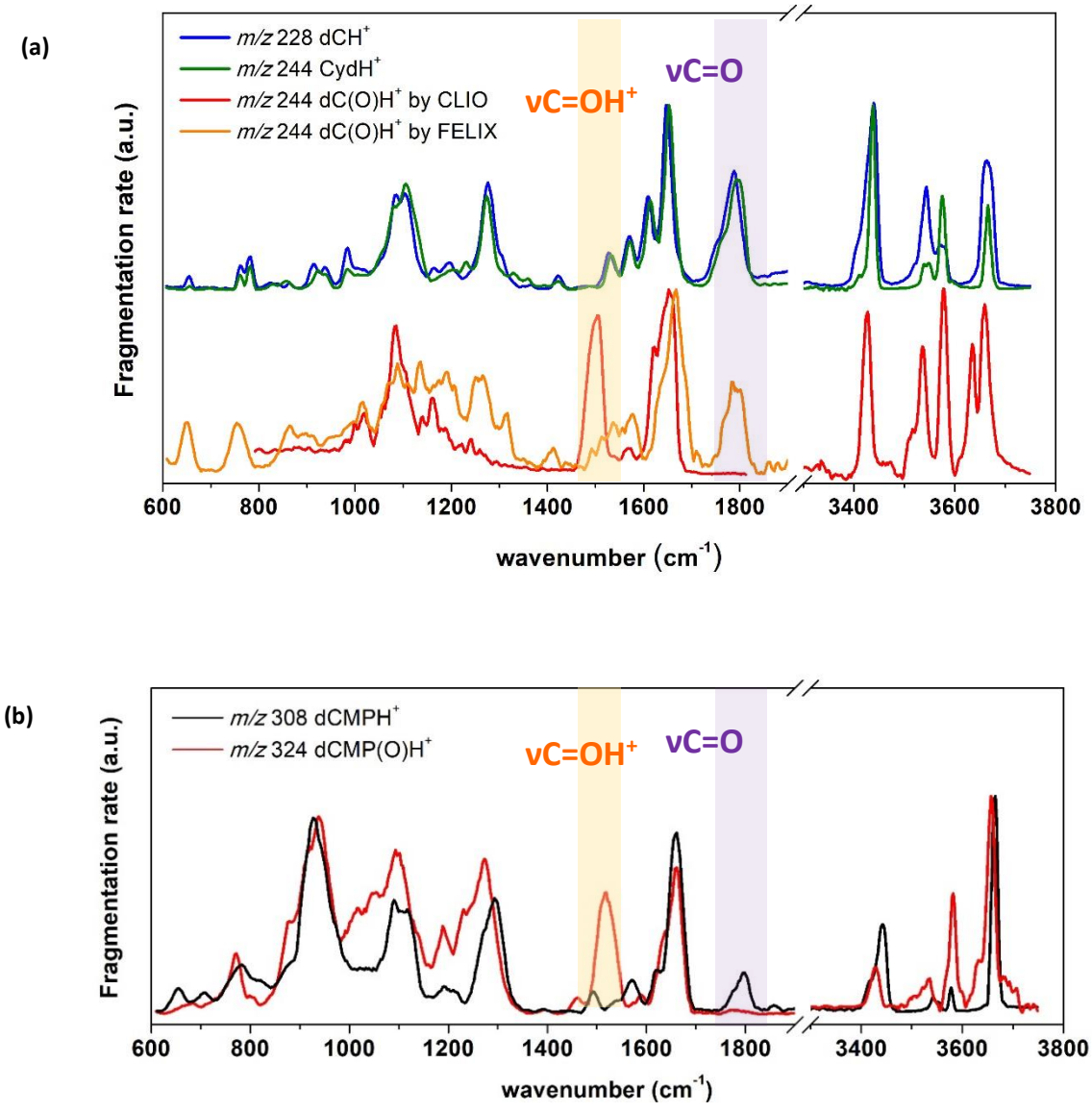

Figure 5. Comparison of the IRMPD spectra for **(a)** dCH^+ (blue), $CydH^+$ (green) and single oxidation product $dC(O)H^+$ (red recorded at CLIO, orange recorded at FELIX); **(b)** $dCMPH^+$ (black) and its single oxidation product $dCMP(O)H^+$ (red).

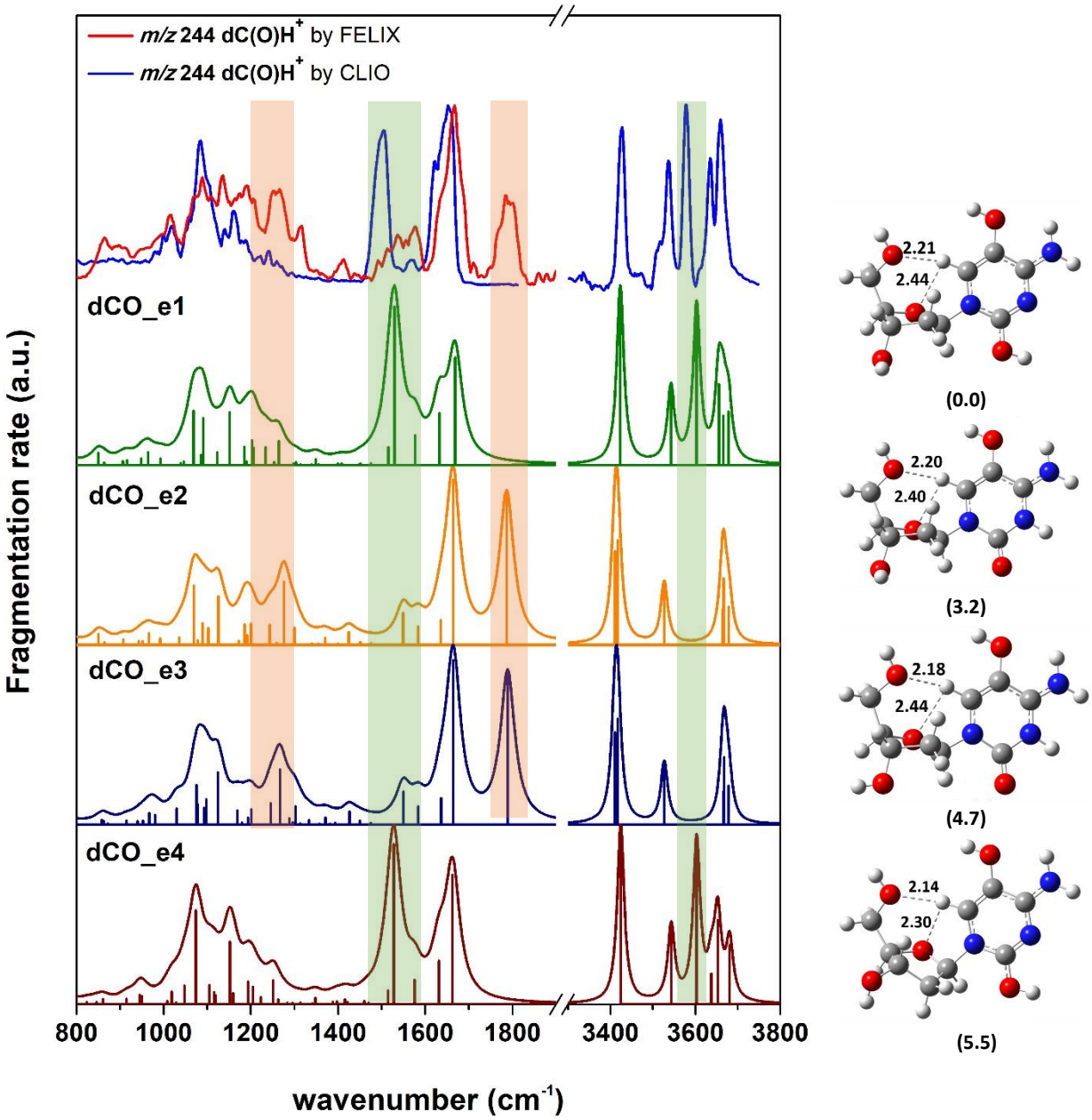

Figure 6. Comparison of the experimental IRMPD spectrum for $dC(O)H^+$ with convoluted calculated IR absorption spectra of representative conformers of the lowest energies optimized at the B3LYP/6-311+G(2d, 2p) level of theory. The H-bond distances are in Å. The corresponding structures are reported on the right. The relative Gibbs free energy (ΔG) at 298 K, in parentheses, is given in kJ/mol.

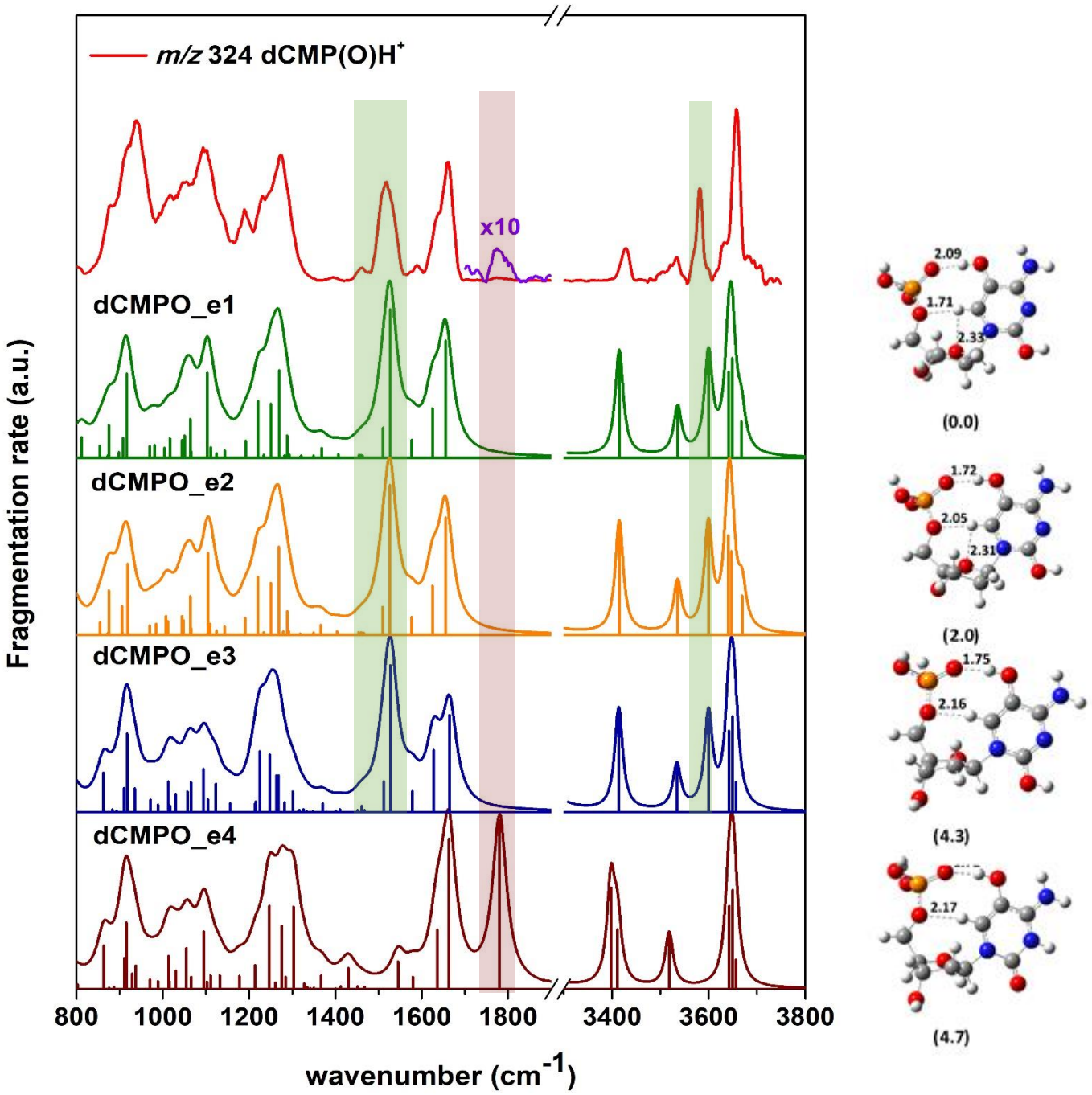

Figure 7. Comparison of the experimental IRMPD spectra for $dC(O)H^+$ with convoluted calculated IR absorption spectra of representative conformers of the lowest energies optimized at the B3LYP/6-311+G(2d,2p) level of theory. The H-bond distances are in Å. The corresponding structures are reported on the right. The relative Gibbs free energy (ΔG) at 298 K in parentheses is given in kJ/mol.

TOC

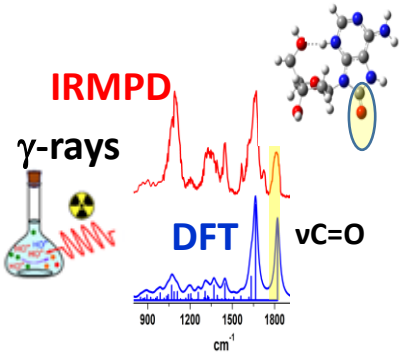

Oxidative lesions in DNA model systems, induced by $OH^{\bullet}$, have been structurally characterized by Infrared Multiple Photon Dissociation (IRMPD) spectroscopy and DFT calculations. The addition of one oxygen atom occurs on the nucleobase moiety.